Chinese Journal of Structural Chemistry

ARTICLE

Enhanced Photothermal Selective Conversion of CO_2 to CH_4 in Water Vapor over Rod-Like Cu and N Co-Doped TiO_2

Ji-Chao Wang[1,3], Xiu Qiao[1], Weina Shi[2]*, Huiling Gao[1]* and Lingchen Guo[1]

[1]*College of Chemistry and Chemical Engineering, Henan Institute of Science and Technology, Xinxiang 453000, China*
[2]*School of Chemistry and Materials Engineering, Xinxiang University, Xinxiang 453000, China*
[3]*School of Ecology and Environment, Zhengzhou University, Zhengzhou 450052, China*

ABSTRACT Enhancing catalytic efficiency and selectivity is critical issues for CO_2 conversion. The rod-like Cu/N co-doped TiO_2 samples (Cu/N-TiO_2) were synthesized by the electrospinning-calcination method. The substitutional Cu and interstitial N doping not only enhanced visible-light absorption ability, but also formed the Ti(III) sites. The obviously synergistic effect between the photocatalysis and thermalcatalysis appeared for CO_2 conversion over the 8-Cu/N-TiO_2 catalyst. After 9 h visible-light-illumination at 160 ˚C, the CO, CH_4 and O_2 yields reached 49.7, 1455.1 and 2910.2 μmol/g_{cat}, respectively. In the 7th cycling, the yields of two main CH_4 and O_2 products were slightly down by less than 11.5%, and the selectivity of CH_4 product kept above 98%. Combined with the theoretical surface mode, Cu/N co-doping could promote the adsorption-ability for H_2O and CO_2 molecules and reduce activation-energy for CO_2 conversion. Hence, the co-doping construction showed a great significance of designing efficient photothermal catalysts for the CO_2 conversion application.

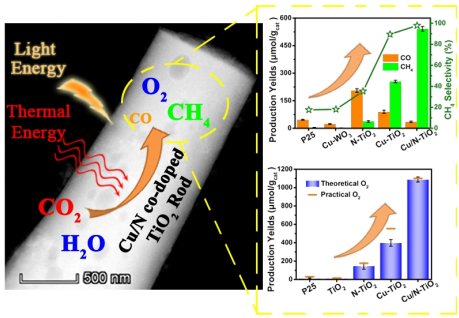

Keywords: CO_2 conversion, photothermal catalysis, rod-like,TiO_2, co-doped

n INTRODUCTION

Photocatalytic reduction of CO_2 into chemical fuels provided an attractive option to ameliorate global warming and help solve the energy crisis.[1-3] One of the challenges is the development of efficient photocatalysts. TiO_2 has received significant attention for photocatalytic CO_2 reduction due to its chemical stability, nontoxicity, and low-cost.[4] However, its wide band gap and rapid recombination of photo-induced carriers limited the practical application of TiO_2 photocatalysts.[5] Moreover, the complex catalytic processes and products cannot be ignored, considering the multiple-electron reduction of CO_2 and the interaction between reactant molecules and surface sites.

In order to overcome the above problems, ongoing attempts have been made to such as nanostructure engineering, element doping, heterojunction construction and surface modification, co-catalyst loading and so on.[6-10] The construction of low dimensional structures such as nanorods, nanoplates and nanotubes could enhance separation and transfer of photoinduced electrons and holes in TiO_2 based catalyst.[6,11-13] D. Regonini et al. reported that the electron transport property of electrospun TiO_2 fibers was higher than that of TiO_2 nanoparticles.[14] Meanwhile, element doping could widen the light-absorption range of TiO_2 based materials and influence the arrangement of surface atoms, leading to the change of catalytic process.[4,11] H. Y. He et al. proved that the N doping narrowed the band gap of N-doped TiO_2 nanorods and nanotubes, resulting in enhanced photocatalytic activities.[15] Meanwhile, the influence of the CO_2 and H_2O adsorption on the selectivity of catalytic products was never ignored. C. Wang et al. reported that the formation of W(V)-O-Ti(III) active sites on TiO_2 surface significantly promoted CO_2 reduction efficiency and selectivity for CH_4 over CO), which exceeds those of pristine TiO_2 by more than one order of magnitude.[16] Therefore, the construction of surface adsorbed sites for CO_2 and H_2O molecules was further studied for CO_2 conversion. Among multitudinous kinds of doped impurities, the effect of Cu atom of semiconductor surface on CO_2 reduction was never neglected.[17-20] M. Park et al. proved that photoexcited electrons by the Cu(I) ions of Cu doped TiO_2 were captured efficiently and transferred to the adsorbed CO_2 molecules[21]. Co-doping method gradually became the focus of TiO_2 based materials for CO_2 photoreduction.[4] The Cu and N co-doped TiO_2 catalysts exhibited superior photocatalytic performances for the degradation of methylene blue, 4-nitrophenol, oxytetracycline or sulfamethoxazole.[22-26] Therefore, the Cu and N co-doped TiO_2 nanorod may become an ideal visible-light-driven catalyst for CO_2 reduction.

Photothermal catalysis is another promising technology to improve catalytic performance of CO_2 reduction due to synergetic effect of photocatalysis and thermalcatalysis.[27-29] The thermal energy promotes the photocatalytic process by reducing the apparent activation energy of photocatalysis, promoting the transfer of charge carriers and mass transfer of reactant.[30] Besides, the reaction rate increases with increasing temperature based on the Arrhenius equation[31]. Stable CO_2 molecules can be activated using additional thermal energy, accelerating the reduction rate of adsorbed CO_2 molecules on the catalyst's surface.[27,28,31] Z. Liu et al. employed the TiO_2 photonic crystals with photothermal effect achieving high efficiency for CO_2 reduction[32]. X. Zhang et al. reported the modification of TiO_2 with cocatalyst and oxygen vacancies for photothermalcatalytic reduction of CO_2 with H_2O steam.[33] C. Wang et al. synthesized TiO_2 catalyst with rich oxygen vacancies followed by hydrogen doping exhibiting improved activity for

DOI: 10.14102/j.cnki.0254-5861.2022-0191

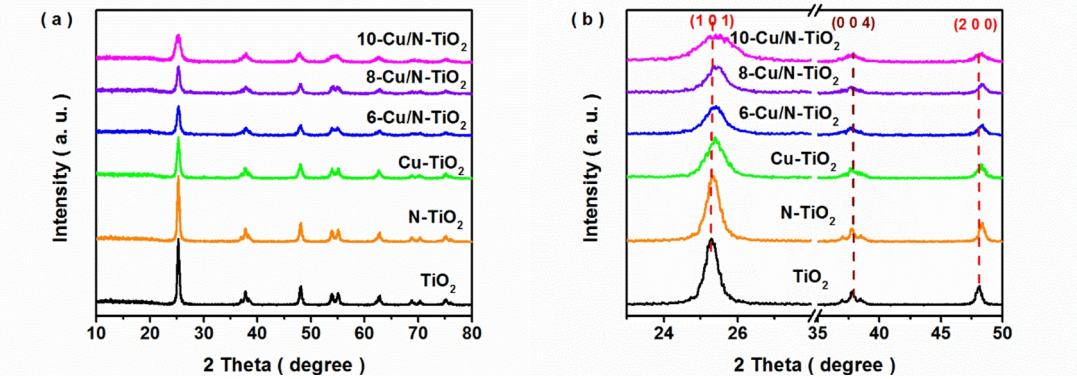

Figure 1. XRD patterns of the obtained samples (degree range: a. 10-80° and b. 23-50°).

photo- and photothermal-catalytic CO_2 reduction.[34] Based on the above considerations, the development of doped TiO_2 catalyst is feasible for efficient photothermal CO_2 conversion.

In this work, Cu and N co-doped TiO_2 nanorods were synthesized by the electrospinning-calcination method for catalytic CO_2 reduction with water vapor. The influence of Cu and N doping on the inherent property of TiO_2 was studied. Photocatalytic and photothermal catalytic activities of CO_2 reduction were investigated over the Cu and N co-doped TiO_2 nanorods. Finally, the surface mode of TiO_2 (1 0 1) facet was built, and the absorbed mechanism of CO_2 and H_2O molecules on the surface was discussed.

n RESULTS AND DISCUSSION

Structure and Morphology. The phase structures of the obtained samples were measured by powder XRD techniques, and the results are shown in Figure 1a. The obvious peaks at 25.3, 37.8, 48.1, 53.9 and 55.1° were corresponding to (1 0 1), (0 0 4), (2 0 0), (1 0 5) and (2 1 1) facets of anatase phase TiO_2. The peak intensity in all doped samples obviously weakened in the existence of Cu dopant, which was the influence of impurity ions on the crystal structure. Although no other diffraction peak of co-doped sample appeared, the (1 0 1) and (2 0 0) peak location of Cu/N codoped TiO_2 evidently moved in high-angle region and the (0 0 4) peak location reversely shifted, compared with the undoped TiO_2 samples. Based on the Bragg's Law and the formula for a tetragonal unit cell, the lattice parameters of the as-prepared samples are summarized in Table S1. The related lattice parameters (*a* and *c*) of Cu-TiO_2 reached 3.826 and 9.617 Å, which are slightly bigger than those of undoped TiO_2 (*a* = 3.815 and *c* = 9.611 Å). It was reasonable since the radius of Cu(I/II) (~0.73 Å) was greater than that of Ti(IV) (0.61 Å), resulting in the extension of bond lengths and the expansion of lattice.[35] Besides, the lattice parameter c value of N-TiO_2 increased by about 0.03 Å and other parameter are never distinctly changed, compared with that of the undoped TiO_2. Combined with the above results, it was consistent with swelling of the unit cell caused by the interstitial N and substitutional Cu in anatase phase TiO_2 structure[35,36].

The surface chemical states of the materials were detested by the XPS measurement. As shown in Figure 2a, the strong peaks at 458.7 and 464.5 eV were assigned to Ti(IV), while the shoulder peaks at 457.4 and 463.1 eV were interpreted as Ti(III) in the 8-Cu/N-TiO_2 sample.[37,38] In the Cu 2p XPS spectrum (Figure 2b), the strong peaks at 934.7 and 954.3 eV were assigned to the Cu(II) in 8-Cu/N-TiO_2.[25] In the spectrum of N 1s (Figure 2c), the characteristic peak of N-O bond appeared at 400.1 eV, indicating that the N impurity was interstitially doped in the lattice of TiO_2.[25,39] Based on the above results, the N and Cu impurities were successfully co-doped into the crystal structure of TiO_2.

The morphologies of TiO_2, N-TiO_2, Cu-TiO_2 and 8-Cu/N-TiO_2 samples were detected by SEM measurement. The SEM image in Figure 3a revealed that TiO_2 exhibited a fibrous morphology. In the images of doped TiO_2 samples (Figure 3b-d), the short rod-like structure appeared due to the impurity doping. The morphology of 8-Cu/N-TiO_2 sample was further elucidated using TEM

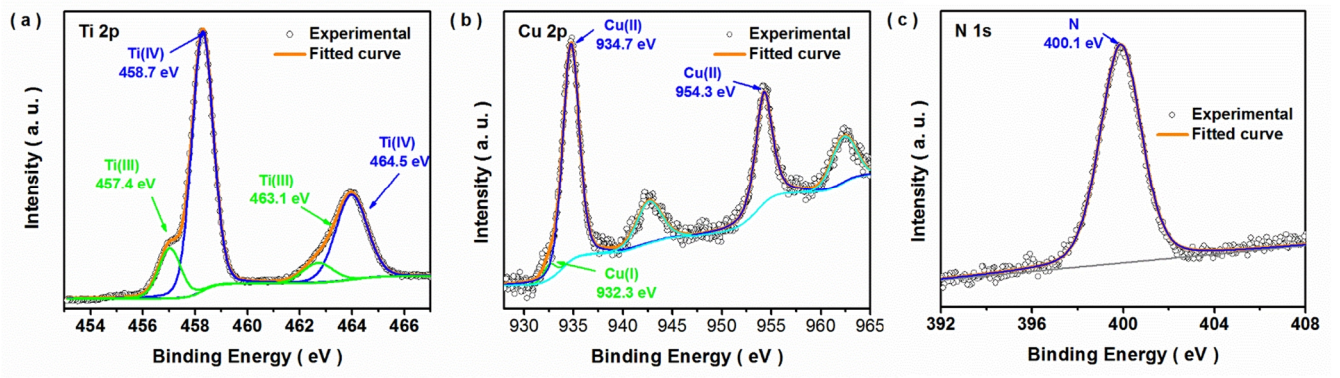

Figure 2. XPS spectra of the 8-Cu/N-TiO_2 sample (a. Ti2p, b. Cu 2p and c. N 1s).

DOI: 10.14102/j.cnki.0254-5861.2022-0191

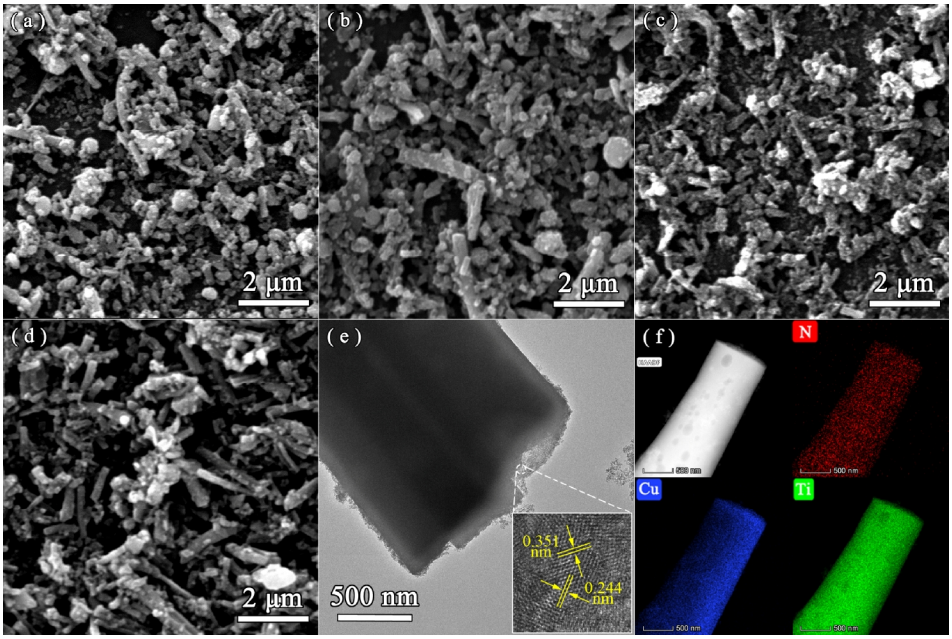

Figure 3. SEM images of the TiO_2 (a), N-TiO_2 (b), Cu-TiO_2 (c) and 8-Cu/N-TiO_2 (d) samples; TEM image (e) and EDX mapping (f) of 8-Cu/N-TiO_2.

measurement. As shown in Figure 3e, the rod-like morphology is made up of nanoparticles. According to the N_2 adsorption-desorption measurements, the surface areas of TiO_2, N-TiO_2, Cu-TiO_2 and 8-Cu/N-TiO_2 samples reached 35.6, 38.6, 36.5 and 45.9 m^2/g, respectively, indicating the Cu and N co-doping promoted the specific surface area of TiO_2 catalyst. In the inset image of Figure 3e, the lattice fringes of 0.351 and 0.244 nm corresponded to the (1 0 1) and (1 0 3) lattice planes of anatase TiO_2. Additionally, the EDX mapping in Figure 3f showed that the N, Cu and Ti elements were uniformly distributed of the rod surface. Combined with the analysis of XRD and XPS, it can be deduced that Cu and N impurities were successfully doped into the rod-like TiO_2 materials.

The DRS and VB-XPS measurements were performed to investigate the band structure of the as-prepared TiO_2, N-TiO_2, Cu-TiO_2 and 8-Cu/N-TiO_2 samples. As shown in Figure 4a, the doped TiO_2 samples exhibited red shift of the absorption edges compared with that of pristine TiO_2. The optical absorption intensity of 8-Cu/N-TiO_2 obviously improved in the wavelength region of 550-800 nm, which was possibly due to the formation of Ti(III) or oxygen defect. In the inset of Figure 4a, the band gap (*E*g) values of TiO_2, N-TiO_2, Cu-TiO_2 and 8-Cu/N-TiO_2 were calculated by the Kubelka-Munk function to be 2.98, 2.79, 2.87 and 2.64 eV, respectively. The decreased *E*g values were induced by Cu and N doping. In the VB-XPS spectra (Figure 4b), the VB values of TiO_2, N-TiO_2, Cu-TiO_2 and 8-Cu/N-TiO_2 samples reached 2.80, 2.68, 2.47 and 2.35 eV, respectively. Combined with *E*g, the corresponding CB values were respectively calculated to be -0.18, -0.19, -0.31 and -0.29 eV. Based on the above results, N and Cu doping promoted the CB position of TiO_2-based catalysts, which was beneficial for CO_2 reduction.

Photocatalytic and Photothermal Catalytic Performance for CO_2 Reduction. The photocatalytic activities of the as-prepared samples were evaluated for CO_2 reduction with H_2O vapor (λ > 400 nm) at room temperature. Firstly, no products were detected in the blank test without catalyst or illumination (Figure S1). As shown in Figure 5a and S3, CO and CH_4 products were found in the gas phase for all catalysts after 3 h of illumination. The photo-

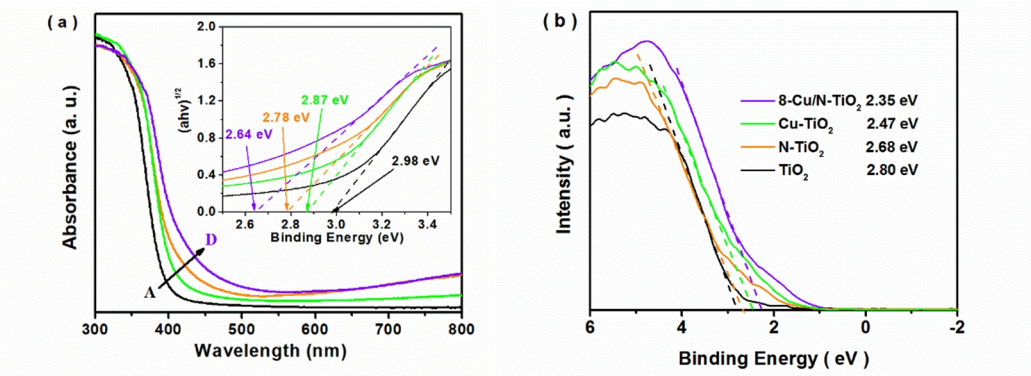

Figure 4. DRS (a) and VB-XPS (b) spectra of the as-prepared samples (A. TiO_2, B. Cu-TiO_2, C. N-TiO_2 and D. 8-Cu/N-TiO_2).

DOI: 10.14102/j.cnki.0254-5861.2022-0191

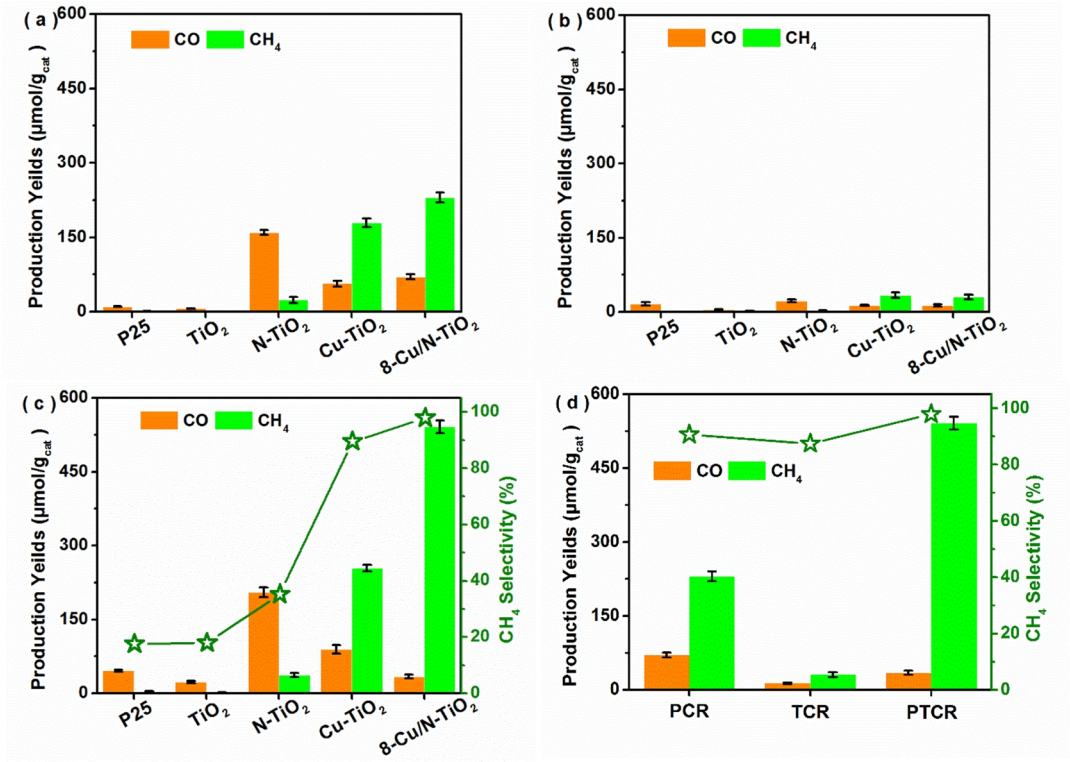

Figure 5. (a) Production yields of photocatalytic (a, visible-light illumination), (b) thermal catalytic (b, 160 °C) and photothermal catalytic (c, 160 °C and visible-light illumination) for CO_2 reduction over different samples after 3 h; (d) comparison of catalytic performance of 8-Cu/N-TiO_2 in the above different catalytic systems.

catalytic activities of the doped TiO_2 catalysts were higher than that of pristine TiO_2, and the CH_4/CO ratio was increased by Cu doping. With increasing the doped Cu content, the yields and CH_4 selectively were all enhanced and the 8-Cu/N-TiO_2 sample exhibited higher activity than other samples (Figure S2a). Although, due to the high overpotential for H_2O oxidation, the practical O_2 yields were lower than the theoretical values, the difference between them became small with the co-existence of illumination and heating (Figure S2b). Thermal catalytic performance (Figure 5b) at 160 °C for all the as-prepared samples showed obvious decreased CO and CH_4 production yields compared with those of photocatalysis. Photothermal catalytic performance in Figure 5c revealed that the CO, CH_4 and O_2 yields of 8-Cu/N-TiO_2 at 160 °C with illumination reached 34.4, 541.4 and 1087.7 μmol/g_{cat}, respectively, and the CH_4 selectivity reached more than 95%. Moreover, the photothermal catalytic activities of all the doped TiO_2 samples were promoted compared with those of undoped TiO_2 and commercial P25, indicating the positive influence of Cu and N co-doping on the catalytic activity. Figure 5d showed the comparison of catalytic performance of Cu/N-TiO_2 in the above different catalytic systems. Catalytic activity and CH_4 selectivity in the photothermal catalytic system were obviously superior to those in thermal and photothermal catalytic systems for the 8-Cu/N-TiO_2 sample, indicating the synergistic effect of heating and illumination for CO_2 reduction. Photocatalytic or photothermalcatalytic performances of TiO_2 based materials for CO_2 reduction have

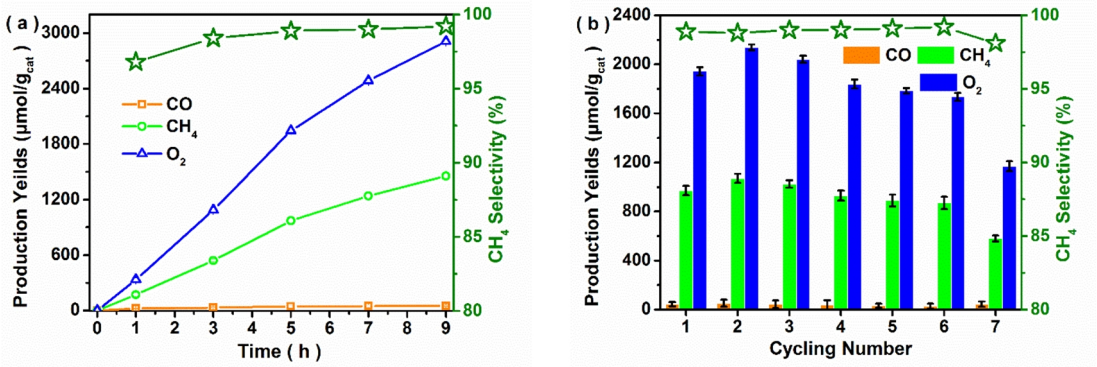

Figure 6. (a) CO, CH_4 and O_2 yields as a function of time over 8-Cu/N-TiO_2; (b) cycling test of photothermalcatalytic CO_2 reduction for the 8-Cu/N-TiO_2 catalyst (5 h for one cycle).

Chin. J. Struct. Chem. **2022**, 41, 2212033-2212042
DOI: 10.14102/j.cnki.0254-5861.2022-0191

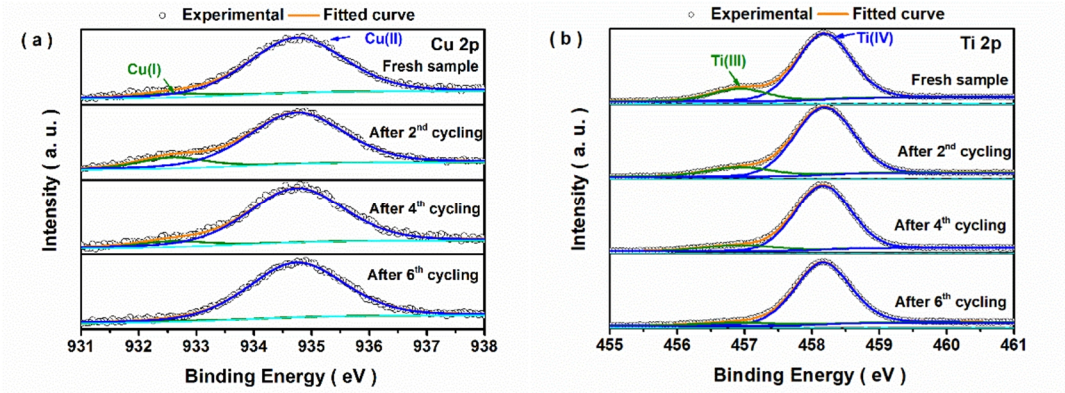

Figure 7. XPS spectra of (a) Cu 2p and (b) Ti 2p for the 8-Cu/N-TiO_2 catalyst before and after cycling tests of photothermalcatalytic CO_2 reduction.

been summarized in Table S2 based on previous studies. The CO, CH_4 and O_2 yields over Cu/N-TiO_2 were obviously higher than those of the reported materials. Additionally, the photothermal catalytic performance under different light conditions in Table S3 showed that high CH_4 selectivity was kept, indicating its independence of wavelength ranges and intensities. Additionally, the difference between the theoretical and practical O_2 yields (Figure S3) of Cu/N-TiO_2 observably fallen off under 160 °C temperature. The influence of catalytic temperature on the photothermal catalytic activity of the 8-Cu/N-TiO_2 sample was further studied and the results are shown in Figure S4. The CO and CH_4 yields firstly increased with the increase of temperature from room temperature (RT) to 160 °C, beyond which the yields gradually decreased (Figure S5a), which may be due to the decrease of CO_2 or H_2O adsorption capacity at high temperature. The practical O_2 yields increased with increasing temperature (Figure S4b) and reached the maximum at 160 °C, indicating that the relatively high temperature had a positive effect on the O_2 generation from H_2O molecules. To further confirm the speculation, H_2O-TPD measurement was recorded. In Figure S5, the adsorbed water interacting with catalyst surface would be desorbed at relatively high temperature (> ~167 °C), thus leading to the decreased catalytic performance of CO_2 conversion.

The photothermalcatalytic activity of 8-Cu/N-TiO_2 was further evaluated by the time-dependent CO_2 reduction behaviors. As shown in Figure 6a, the CO and CH_4 yields increased linearly by prolonging the irradiation-heating time. After 9 h of continuous reaction, the CO, CH_4 and O_2 yields reached 49.7, 1455.1 and 2910.2 μmol/g_{cat}, respectively. The stability of the photocatalyst played an important role in practical application. In this study, cycling experiments for photothermal catalytic CO_2 reduction were carried out with each period lasting 5 h and the result is shown in Figure 6b. The CO, CH_4 and O_2 yields still reached 28.4, 870.5 and 1735.7 μmol/g_{cat} in the 6th cycling experiment. To further investigate the stability, XRD patterns of 8-Cu/N-TiO_2 before and after seven cycles is shown in Figure S6. No apparent change was found after cycling experiments, suggesting that 8-Cu/N-TiO_2 possesses an excellent stability without structural deterioration during the CO_2 reduction process.

XPS analysis was conducted to investigate the surface chemical states of the 8-Cu/N-TiO_2 catalyst in the cycling test, and the results are presented in Figure 7 and Table S4. The area ratio of characteristic peak for Cu(I) and Cu(II) was related to the content ratio of Cu(I) and Cu(II) on the surface. The calculated Cu(I)/Cu(II) ratios after three cycling tests increased as compared with that of the fresh sample, and the ratio slightly decreased after the 4th cycling experiment. The variation trend of Cu(I)/Cu(II) ratio was consistent with that of photothermal catalytic activity. It was indicated that the enhanced catalytic activity was mainly caused by the existence of Cu(I) compared with the Cu(II) impurity in the doped TiO_2 sample.[19,40] Meanwhile, the Ti(III)/Ti(IV) ratio on the surface decreased after the cycling tests. There were no obvious differences of N 1s characteristic peaks between the used and fresh samples (Figure S7). Hence, the Cu(I) and Ti(III) impurities evidently influenced the catalytic activity of CO_2 conversion.

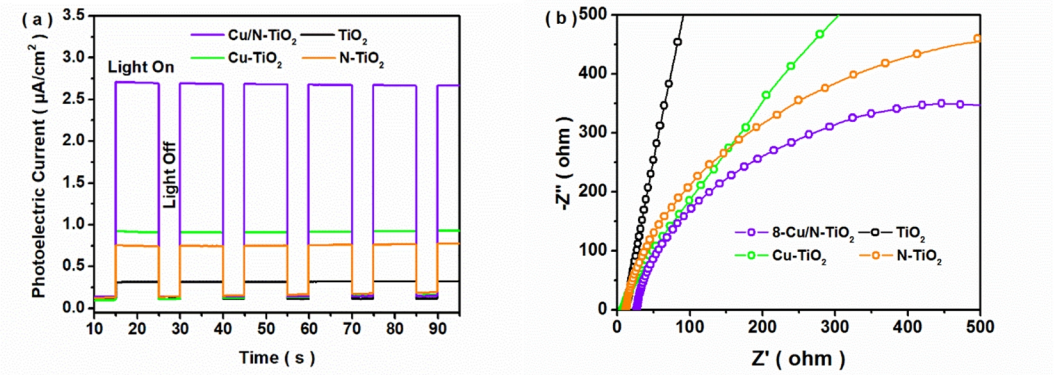

Figure 8. I-t curves (a) and EIS spectra (b) of the obtained samples.

DOI: 10.14102/j.cnki.0254-5861.2022-0191

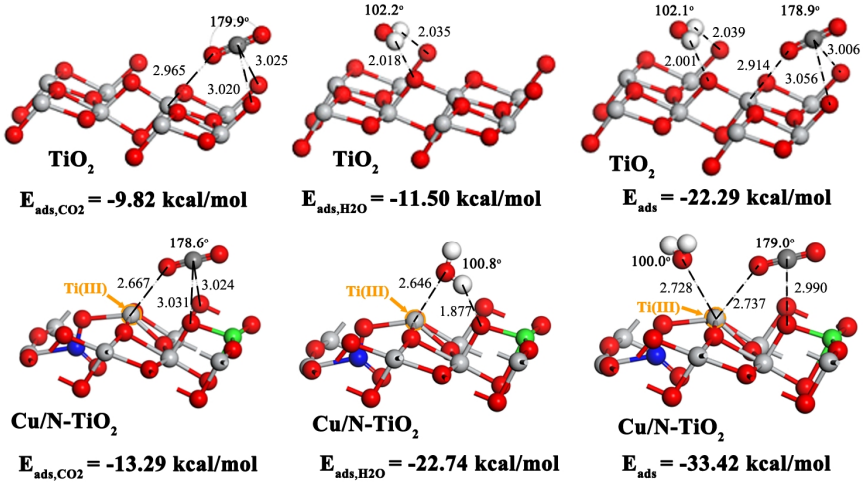

Figure 9. DFT optimized CO_2 adsorption configurations on (1 0 1) facets of pristine TiO_2 and Cu/N-TiO_2. (Bond distance units: Å; Color scheme: Ti, gray; O, red; H, white; C, dark gray; Cu, green; N, blue).

Catalytic Mechanism. The photocurrent response curves of TiO_2, Cu-TiO_2, N-TiO_2 and 8-Cu/N-TiO_2 samples are presented in Figure 8a. The Cu/N-TiO_2 sample exhibited the highest photocurrent intensity under light illumination, which was about 1.5, 15.2 and 1.5 times those of TiO_2, Cu-TiO_2 and N-TiO_2, indicating that Cu and N co-doping improved charge separation of the 8-Cu/N-TiO_2[41]. The radius of the semicircle in the EIS spectra (Figure 8b) followed the order: TiO_2 > Cu-TiO_2 > N-TiO_2 > Cu/N-TiO_2. This suggested that Cu/N-TiO_2 sample had a smaller resistance, facilitating charge transfer at the interface[42]. Therefore, Cu and N co-doping facilitated transfer of photo-induced carriers, leading to the enhanced photocatalytic performance. Combined with XRD results, the exposed (1 0 1) surface of anatase phase TiO_2 was selected, and several models of Cu and N mono-doped TiO_2 have been optimized (Figure S8). According to the formation energy, lattice structure and chemical composition (Figure S8e), two structure modes of N@gap and Cu@Ti_{5c} were adopted for the N and Cu mono-doped TiO_2 samples, and then multi-modes of surface structure for co-doped TiO_2 (Figure S9) were built and optimized. According to enhanced catalytic performance and the chemical composition, the influence of Cu/N impurities and Ti(III) site of TiO_2 surface on the CO_2 conversion was of significance. The co-doped surface mode with the interstitial N and lower state Cu impurities (Cu@Ti_{5c}&N@gap TiO_2 mode) was selected due to the lower formation energy and structural feature (the existence of Ti(III) and N-O bond). As shown in Figure 9 and Figure S10, the adsorption energies of CO_2 (-11.96 kcal/mol) and H_2O (-21.40 kcal/mol) for the Cu and N mono-doped TiO_2 sample decreased compared with those of pristine TiO_2 (-9.82 and -11.50 kcal/mol). Similarly, the above adsorption energies for Cu-TiO_2 noticeably decreased. In the system containing CO_2 and H_2O molecules, the doped Cu and N impurities facilitated adsorption of reactant molecules. In mode of codoped TiO_2 surface (Figure 9), the CO_2 molecule was adsorbed around the doped Cu and N impurities, and its adsorption energy (-13.29 kcal/mol) noticeably decreased compared with that of pristine TiO_2. Similarly, the adsorption energy of H_2O molecule on Cu/N-TiO_2 surface (-22.74 kcal/mol) was obviously lower than that of TiO_2 (-11.50 kcal/mol). Additionally, it is notable that the O=C=O angle in CO_2 and the H-O-H angle in H_2O on the Cu/N co-doped TiO_2 surface reduced to about 178.6° and 100.8°, indicating that the energy barrier for CO_2 and H_2O activation was obviously lower than that of TiO_2. To further confirm the above speculation, the adsorption abilities of undoped and codoped TiO_2 samples were measured, with the results shown in Figure S11. The CO_2 and H_2O adsorption capacities of the co-doped TiO_2 sample were higher than those of undoped TiO_2, which agreed with the theoretical results of surface mode. Considering the simultaneous process of CO_2 reduction and H_2O oxidization, the adsorption of co-existed CO_2 and H_2O molecules was studied on the catalyst surface. H_2O and CO_2 molecules were adsorbed around the Ti(III) site on surface, and their distance was distinctly shortened (Figure S12). The adsorbed energy (-33.42 kcal/mol) in the CO_2 and H_2O co-existed system was lower than that of undoped TiO_2 (-22.29 kcal/mol). Additionally, the angle of H-O-H in reactant molecules on the Cu/N-TiO_2 surface still exhibited a descent in the co-existence of CO_2 and H_2O by comparison with that of pristine TiO_2 surface. Based on the above results, the substitutional doped Cu and N impurities could effectively promote the adsorption ability for CO_2 and H_2O molecules, leading to the enhanced catalytic performance.

According to the enhanced catalytic performance for CO_2 conversion, the doped Cu and N impurities of TiO_2 catalyst could promote the adsorption ability for H_2O and CO_2 molecules. Meanwhile, the symmetry of adsorbed reactant molecules on the surface of Cu/N-TiO_2 surface dropped off, compared with that of the pristine TiO_2, resulting in the enhanced catalytic activity for CO_2 reduction. For further exploring the CO_2 conversion on the surface, the in situ diffuse reflectance infrared Fourier transform spectra (DRIFTS) were recorded. In Figure 10a, several characteristic peaks of CO_3^{2-} (1318 and 1365 cm^{-1}), CO_2^- (1650, 1516 and 1222 cm^{-1}), HCO_3^- (1626 and 1422 cm^{-1}) and $HCOO^-$ (1541 and 1339 cm^{-1}) species appeared, and the peak intensities gradually in-

DOI: 10.14102/j.cnki.0254-5861.2022-0191

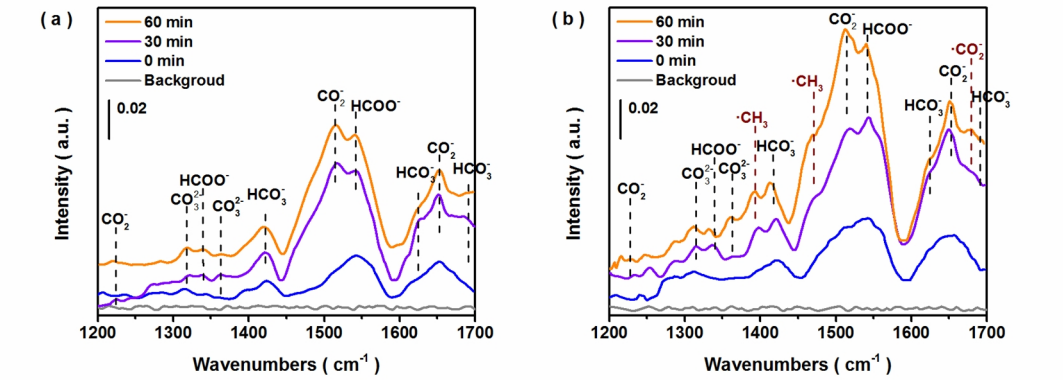

Figure 10. DRIFTS spectra of the undoped TiO_2 (a) and 8-Cu/N-TiO_2 samples.

creased with increasing the light irradiation time[43-48]. It was demonstrated that $HCOO^-$ is an important intermediate during the process of photocatalytic CO_2 reduction to CO, consistent with previous reports[47,48]. The above peaks also appeared with 8-Cu/N-TiO_2 sample and their peak intensity is higher than that of undoped TiO_2, resulting in higher CO_2 conversion efficiency over Cu/N codoped TiO_2. Particularly, three new peaks of $\cdot CH_3$ (1458 and 1389 cm^{-1}) and $\cdot CO_2^-$ (1679 cm^{-1}) were identified for the 8-Cu/N-TiO_2 sample compared with the undoped TiO_2[49,50]. The characteristic peaks of $\cdot CH_3$ indicated the production of CH_4, which agreed well with the product selectivity of 8-Cu/N-TiO_2. Additionally, the peaks of partial species ($\cdot CH_3$, $HCOO^-$, HCO_3^- and so on) slightly shifted due to the variation of surface charge for the catalysts[47]. According to the DRIFTS results (Figure 10) and catalytic performance, the activation of CO_2 to $\bullet CO_2^-$ was achieved by shoving excessive photo-induced electrons to the adsorbed CO_2 molecules at the surface defect sites[51]. $HCOO^-$ was taken as an intermediate to generate CO selectively in photocatalytic CO_2 conversion[52]. HCO_3^- species, generated from CO_2 and OH groups, served as a possible intermediate for the production of CO and C1 fuels associated with the emergence of dissociative H atoms[52]. Both CO_3^{2-} and HCO_3^- were important intermediates, which were subsequently transformed into CO products[53,54]. The characteristic peaks of methyl radicals ($\bullet CH_3$) indicated the production of CH_4[50]. Hence, the possible mechanism of CO_2 conversion with water vapor was summarized as follows:

$$\text{catalyst} + E \rightarrow h^+ + e^- \quad (1)$$
$$H_2O + h^+ \rightarrow \bullet OH + H^+ \quad (2)$$
$$H_2O + 2h^+ \rightarrow H_2O_2 + 2H^+ \quad (3)$$
$$H_2O_2 + E \rightarrow 2H_2O + O_2(g) \quad (4)$$
$$CO_2 + e^- \rightarrow \bullet CO_2^- \quad (5)$$
$$\bullet CO_2^- + \bullet OH \rightarrow HCO_3^- \quad (6)$$
$$HCO_3^- + H^+ + 2e^- \rightarrow 2OH^- + CO(g) \quad (7)$$
$$CO_3^{2-} + 2H^+ + 2e^- \rightarrow 2OH^- + CO(g) \quad (8)$$
$$\bullet CO_2 + H^+ + e^- \rightarrow \bullet COOH \quad (9)$$
$$\bullet COOH + H^+ + e^- \rightarrow \bullet CO + H_2O \quad (10)$$
$$\bullet CO \rightarrow CO(g) \quad (11)$$
$$\bullet COOH + H^+ + e^- \rightarrow \bullet HCOOH \quad (12)$$
$$\bullet HCOOH + H^+ + e^- \rightarrow \bullet CHO + H_2O \quad (13)$$

n CONCLUSION

The rod-like Cu/N co-doped TiO_2 samples were synthesized by the electrospinning-calcination method. The visible-light absorption ability of catalyst was enhanced by the substitutional Cu and interstitial N doping and the Ti(III) formation was discovered in co-doped sample. The synergistic effect between the photocatalysis and thermalcatalysis was discovered for CO_2 conversion over 8-Cu/N-TiO_2. After constant catalytic conduction for 9 h, the CO, CH_4 and O_2 yield can reach 49.7, 1455.1 and 2910.2 μmol/g_{cat}. In the 7th cycling experiment, the yields of two main products (CH_4 and O_2) were slightly down by less than 11.5%. The surface mode of the main (1 0 1) crystal face over Cu/N co-doped TiO_2 was constructed. Based on the experimental and theoretical results, Cu/N co-doping not only was in favor of the CO_2 and H_2O adsorption, but also reduced activation energy for CO_2 reduction process.

n EXPERIMENTAL

Synthesis of Cu/N-TiO_2. The rod-like TiO_2 samples were synthesized by the electrospinning-calcination method. Typically, 3.4 mL butyl titanate and 3.0 g polyvinyl pyrrolidone were dissolved into 15 mL ethyl alcohol. The TiO_2 precursor was obtained by electrostatic spinning under the voltage of 18.5 kV with a distance of 10 cm between the needle and acceptor. And then, the undoped TiO_2 sample was obtained after calcination at 580 ˚C for 1 h. Cu doped TiO_2 was synthesized by the above method with the addition of 0.2 g $Cu(NO_3)_2 \cdot 3H_2O$, which was named as Cu-TiO_2. N doped TiO_2 (N-TiO_2) was synthesized similarly by adding 15 mL dimethyl formamide instead of ethyl alcohol. N and Cu co-doped TiO_2 was synthesized similarly with the addition of $Cu(NO_3)_2 \cdot 3H_2O$ and 15 mL dimethyl formamide, which was finally named as *x*-Cu/N-TiO_2 (*x* was on behalf of ideal amount-of-substance ratio of Cu/Ti in raw materials). The contents of metal ions for all of the obtained samples were detected by ICP-AES measurements, and the real Cu/Ti ratios (Table S5) in the composites were basically consistent with the initial inventory ratio.

Characterization. The structure and composition characterization of the obtained samples were explored using X-ray diffractometer (XRD), scanning electron microscope (SEM), transmission electron microscopy (TEM), X-ray photoelectron spectroscopy (XPS), UV-Vis diffuse reflectance spectra (DRS), photoelectrochemical test, in situ diffuse reflectance infrared Fourier transform spectra (DRIFTS) and so on. The processes of the

DOI: 10.14102/j.cnki.0254-5861.2022-0191

above measurements and tests were detailed in Supporting Information S1.

Catalytic Test for CO_2 Reduction. Photocatalytic, thermal and photothermal catalytic performances for CO_2 reduction were measured in a 250 mL pressure-proof reactor (CEL-HPR250T, Beijing China Education Au-Light Co., LTD, China). The dispersion containing 15 mg catalyst and 5 mL H_2O drop onto a hydrophilic porous quatz plate (2.8cm × 2.8cm). After vacuum drying at 110 °C, the plate loaded with sample was put into the reactor and subsequently vacuum-treated. Before illumination, high purity CO_2 (99.995%) as the purging gas was injected into the reactor for several times, and the reactant mixture (CO_2 and H_2O vapor) was generated by the flowing CO_2 gas and water bubbler. Thermal catalytic CO_2 reduction was conducted at the predetermined temperature (160 °C). Photothermal catalytic performance for CO_2 reduction was investigated at 160 ˚C, and a 300 W Xe lamp with an ultraviolet cutoff filter (λ > 400 nm) was adopted as the light source. For comparison, photocatalytic performance for CO_2 reduction was evaluated at low temperature (3 ˚C), and all the other conditions remained unchanged. The gaseous products (CO, O_2 and CH_4) from the reactor were quantifiably identified for off-line analysis using a gas chromatograph (GC-7890II Beijing China Education Au-Light Co., LTD, China) with FID and TCD detectors, and the other hydrocarbon was further analyzed by GC-MS (Agilent 7890A-5975C) equipped with a DB-FFAP capillary column.

The selectivity of CO (S_{CO}) and CH_4 (S_{CH4}) products and the theoretical O_2 yield ($Y_{ideal\ O2}$) were obtained according to Equation (14), (15) and (16), respectively:

$$S_{CO} = 2\times n_{CO}/(2\times n_{CO} + 8\times n_{CH4})\times 100\% \quad (14)$$

$$S_{CH4} = 8\times n_{CH4}/(2\times n_{CO} + 8\times n_{CH4})\times 100\% \quad (15)$$

$$Y_{ideal\ O2} = 0.5\times n_{CO} + 2\times n_{CO} \quad (16)$$

Theoretical Model and Calculation Method. A 48-atom anatase supercell of pure TiO_2 with the I41/AMD space group was constructed and optimized by using the first principle pseudopotential plane wave algorithm of Koho-Sham self-consistent density functional theory with the Castep package of Materials Studio. The geometrically optimized lattice parameters of pure TiO_2 super cell were $a = b = 3.904$ Å, $c = 9.878$ Å, $\alpha = \beta = \gamma = 90^o$, respectively. Based on the optimized geometrical structure of pure TiO_2 supercell, the TiO_2 (1 0 1) surface was modeled with eighteen atomic layers. The terminal atoms of TiO_2 (1 0 1) surface were dicoordinated O atoms. Considering the role of defective sites on the TiO_2 (1 0 1) surface, we also considered six co-doped-TiO_2 models (Figure S9). A vacuum layer of 15 Å was set in the direction perpendicular to the (1 0 1) surface for all the models. Eight atomic layers on the surface were subjected for coordinate relaxation using the Castep package of Materials Studio. The ultra-soft pseudopotential as well as the generalized gradient approximation of Perdew-Burke-Ernzerhof parameterization (GGA-PBE) were applied to approximately describe the interaction between valence electrons and ions. In this work, the cut-off energy of plane wave was set to be 400 eV, and the Monkhorst-Pack scheme with a 2 ×3×1 k-point grid was used to divide the Brillouin zone. During the processes of atomic relaxation calculations, the specific optimization parameters were selected as follows: the convergence value of the total energy of the system was 2.0×10^{-5} eV/atom; The force on each atom was less than 0.05 eV/Å, and the internal stress deviation was less than 0.1 GPa; The maximum displacement between atoms was less than 0.002 Å. The standard DFT could underestimate the band gap of the semiconductors. The DFT+U formalism was thus employed, and the values of parameter U were set to be 8.0 eV for the Ti 3d electrons and 7.5 eV for the Cu 3d electrons.

In order to study the effect of Cu and N doping on the CO_2 and H_2O adsorption capacities, the grand canonical Monte Carlo (GCMC) method via Adsorption Locator was used to adsorb CO_2 and H_2O molecules onto the TiO_2 (1 0 1) surface, and the best adsorption site and configuration were obtained by the simulated annealing methods.

n ACKNOWLEDGEMENTS

This work was supported by the National Natural Science Foundation of China (No. 51802082), Key Scientific and Technological Project of Henan Province (No. 222102320100) and Program for Science & Technology Innovation Talents in Universities of Henan Province (No. 21HATIT016).

n AUTHOR INFORMATION

Corresponding authors. Emails: shiweina516@163.com (Dr. W. Shi) and mzfghl@hist.edu.cn (Dr. H. Gao)

n COMPETING INTERESTS

The authors declare no competing interests.

n ADDITIONAL INFORMATION

Supplementary information is available for this paper at http://manu30.magtech.com.cn/jghx/EN/10.14102/j.cnki.0254-5861.2022-0191

For submission: https://www.editorialmanager.com/cjschem

n REFERENCES

(1) Wu, J.; Huang, Y.; Ye, W.; Li, Y. CO_2 reduction: from the electrochemical to photochemical approach. *Adv. Sci.* **2017**, 4, 1700194.

(2) Wu, J.; Liu, J.; Xia, W.; Ren, Y.-Y.; Wang, F. Advances on photocatalytic CO_2 reduction based on CdS and CdSe nano-semiconductors. *Acta Phys.-Chim. Sin.* **2021**, 37, 2008043.

(3) Qin, Z.; Wu, J.; Li, B.; Su, T.; Ji, H. Ultrathin layered catalyst for photocatalytic reduction of CO_2. *Acta Phys.-Chim. Sin.* **2021**, 37, 2005027.

(4) Abdullah, H.; Khan, M. M. R.; Ong, H. R.; Yaakob, Z. Modified TiO_2 photocatalyst for CO_2 photocatalytic reduction: an overview. *J. CO_2 Util.* **2017**, 22, 15-32.

(5) Habisreutinger, S. N.; Schmidt-Mende, L.; Stolarczyk, J. K. Photocatalytic reduction of CO_2 on TiO_2 and other semiconductors. *Angew. Chem., Int. Ed.* **2013**, 52, 7372-7408.

(6) Lu, N.; Zhang, M.; Jing, X.; Zhang, P.; Zhu, Y.; Zhang, Z. Electrospun semiconductor-based nano-heterostructures for photocatalytic energy conversion and environmental remediation: opportunities and challenges. *Energy Environ. Mater.* **2022**, doi:10.1002/eem2.12338

(7) Zeshan, M.; Bhatti, I. A.; Mohsin, M.; Iqbal, M.; Amjed, N.; Nisar, J.; AlMasoud, N.; Alomar, T. S. Remediation of pesticides using TiO_2 based

DOI: 10.14102/j.cnki.0254-5861.2022-0191

photocatalytic strategies: a review. *Chemosphere* **2022**, 300, 134525.
(8) Kong, L.; Zhang, X.; Wang, C.; Wan, F.; Li, L. Synergic effects of Cu_xO electron transfer co-catalyst and valence band edge control over TiO_2 for efficient visible-light photocatalysis. *Chin. J. Catal.* **2017**, 38, 2120-2131.
(9) Wang, Z.; Fan, J.; Cheng, B.; Yu, J.; Xu, J. Nickel-based cocatalysts for photocatalysis: hydrogen evolution, overall water splitting and CO_2 reduction. *Mater. Today Phys.* **2020**, 15, 100279.
(10) Duan, S.; Wu, S.; Wang, L.; She, H.; Huang, J.; Wang, Q. Rod-shaped metal organic framework structured PCN-222(Cu)/TiO_2 composites for efficient photocatalytic CO_2 reduction. *Acta Phys.-Chim. Sin.* **2020**, 36, 1905086.
(11) Ma, Y.; Qiu, B.; Zhang, J.; Xing, M. Vacancy engineering of ultrathin 2D materials for photocatalytic CO_2 reduction. *ChemNanoMat* **2021**, 7, 368-379.
(12) Pan, R.; Liu, J.; Zhang, J. Defect engineering in 2D photocatalytic materials for CO_2 reduction. *ChemNanoMat* **2021**, 7, 737-747.
(13) Li, Y.; Zhang, W.; Shen, X.; Peng, P.; Xiong, L.; Yu, Y. Octahedral Cu_2O-modified TiO_2 nanotube arrays for efficient photocatalytic reduction of CO_2. *Chin. J. Catal.* **2015**, 36, 2229-2236.
(14) Regonini, D.; Teloeken, A. C.; Alves, A. K.; Berutti, F. A.; Gajda-Schrantz, K.; Bergmann, C. P.; Graule, T.; Clemens, F. Electrospun TiO_2 fiber composite photoelectrodes for water splitting. *ACS Appl. Mater. Interfaces* **2013**, 5, 11747-11755.
(15) He, Z.; He, H. Y. Synthesis and photocatalytic property of N-doped TiO_2 nanorods and nanotubes with high nitrogen content. *Appl. Surf. Sci.* **2011**, 258, 972-976.
(16) Feng, Y.; Wang, C.; Cui, P.; Li, C.; Zhang, B.; Gan, L.; Zhang, S.; Zhang, X.; Zhou, X.; Sun, Z.; Wang, K.; Duan, Y.; Li, H.; Zhou, K.; Huang, H.; Li, A.; Zhuang, C.; Wang, L.; Zhang, Z.; Han, X. Ultrahigh photocatalytic CO_2 reduction efficiency and selectivity manipulation by single-tungsten-atom oxide at the atomic step of TiO_2. *Adv. Mater.* **2022**, 34, 2109074.
(17) Cui, X.; Shi, F. Selective conversion of CO_2 by single-site catalysts. *Acta Phys.-Chim. Sin.* **2021**, 37, 2006080.
(18) Johnson, D.; Qiao, Z.; Djire, A. Progress and challenges of carbon dioxide reduction reaction on transition metal based electrocatalysts. *ACS Appl. Energy Mater.* **2021**, 4, 8661-8684.
(19) Zhang, M.; Cheng, G.; Wei, Y.; Wen, Z.; Chen, R.; Xiong, J.; Li, W.; Han, C.; Li, Z. Cuprous ion (Cu^+) doping induced surface/interface engineering for enhancing the CO_2 photoreduction capability of $W_{18}O_{49}$ nanowires. *J. Colloid Interface Sci.* **2020**, 572, 306-317.
(20) Ola, O.; Maroto-Valer, M. M. Copper based TiO_2 honeycomb monoliths for CO_2 photoreduction. *Catal. Sci. Technol*. **2014**, 4, 1631-1637.
(21) Park, M.; Kwak, B. S.; Jo, S. W.; Kang, M. Effective CH_4 production from CO_2 photoreduction using TiO_2/*x* mol% Cu-TiO_2 double-layered films. *Energy Convers. Manage.* **2015**, 103, 431-438.
(22) Mathis, J. E.; Lieffers, J. J.; Mitra, C.; Reboredo, F. A.; Bi, Z.; Bridges, C. A.; Kidder, M. K.; Paranthaman, M. P. Increased photocatalytic activity of TiO_2 mesoporous microspheres from codoping with transition metals and nitrogen. *Ceram. Int.* **2016**, 42, 3556-3562.
(23) Jaiswal, R.; Bharambe, J.; Patel, N.; Dashora, A.; Kothari, D. C.; Miotello, A. Copper and nitrogen co-doped TiO_2 photocatalyst with enhanced optical absorption and catalytic activity. *Appl. Catal., B* **2015**, 168-169, 333-341.
(24) Isari, A. A.; Hayati, F.; Kakavandi, B.; Rostami, M.; Motevassel, M.; Dehghanifard, E. N. Cu co-doped TiO_2@functionalized SWCNT photocatalyst coupled with ultrasound and visible-light: an effective sono-photocatalysis process for pharmaceutical wastewaters treatment. *Chem. Eng. J.* **2020**, 392, 123685.
(25) Wang, S.; Yang, X. J.; Jiang, Q.; Lian, J. S. Enhanced optical absorption and photocatalytic activity of Cu/N-codoped TiO_2 nanocrystals. *Mater. Sci. Semicond. Process.* **2014**, 24, 247-253.
(26) He, Z. Q.; Jiang L. X.; Han J.; Wen, L. N.; Chen, J. M.; Song, S. Activity and selectivity of Cu and Ni doped TiO_2 in the photocatalytic reduction of CO_2 with H_2O under UV-light irradiation. *Asian J. Chem.* **2014**, 26, 4759-4766.
(27) Sun, M.; Zhao, B.; Chen, F.; Liu, C.; Lu, S.; Yu, Y.; Zhang, B. Thermally-assisted photocatalytic CO_2 reduction to fuels. *Chem. Eng. J.* **2021**, 408, 127280.
(28) Li, Z.; Zhang, L.; Huang, W.; Xu, C.; Zhang, Y. Photothermal catalysis for selective CO_2 reduction on the modified anatase TiO_2 (101) surface. *ACS Appl. Energy Mater.* **2021**, 4, 7702-7709.
(29) Xie, B.; Lovell, E.; Tan, T. H.; Jantarang, S.; Yu, M.; Scott, J.; Amal, R. Emerging material engineering strategies for amplifying photothermal heterogeneous CO_2 catalysis. *J. Energy Chem*. **2021**, 59, 108-125.
(30) Zhang, F.; Li, Y.-H.; Qi, M.-Y.; Yamada, Y. M. A.; Anpo, M.; Tang, Z.-R.; Xu, Y.-J. Photothermal catalytic CO_2 reduction over nanomaterials. *Chem Catal.* **2021**, 1, 272-297.
(31) Wang, S.; Tountas, A. A.; Pan, W.; Zhao, J.; He, L.; Sun, W.; Yang, D.; Ozin, G. A. CO_2 footprint of thermal versus photothermal CO_2 catalysis. *Small* **2021**, 17, 2007025.
(32) Low, J.; Zhang, L.; Zhu, B.; Liu, Z.; Yu, J. TiO_2 photonic crystals with localized surface photothermal effect and enhanced photocatalytic CO_2 reduction activity. *ACS Sustain. Chem. Eng.* **2018**, 6, 15653-15661.
(33) Li, Y.; Wang, C.; Song, M.; Li, D.; Zhang, X.; Liu, Y. TiO_{2-x}/CoO_x photocatalyst sparkles in photothermocatalytic reduction of CO_2 with H_2O steam. *Appl. Catal., B* **2019**, 243, 760-770.
(34) Yu, F.; Wang, C.; Li, Y.; Ma, H.; Wang, R.; Liu, Y.; Suzuki, N.; Terashima, C.; Ohtani, B.; Ochiai, T.; Fujishima, A.; Zhang, X. Enhanced solar photothermal catalysis over solution plasma activated TiO_2. *Adv. Sci.* **2020**, 7, 2000204.
(35) Yang, X.; Cao, C.; Hohn, K.; Erickson, L.; Maghirang, R.; Hamal, D.; Klabunde, K. Highly visible-light active C- and V-doped TiO_2 for degradation of acetaldehyde. *J. Catal.* **2007**, 252, 296-302.
(36) He, J.; Liu, Q.; Sun, Z.; Yan, W.; Zhang, G.; Qi, Z.; Xu, P.; Wu, Z.; Wei, S. High photocatalytic activity of rutile TiO_2 induced by iodine doping. *J. Phys. Chem. C* **2010**, 114, 6035-6038.
(37) Wang, P.; Jia, C.; Li, J.; Yang, P. Ti^{3+}-doped TiO_2(B)/anatase spheres prepared using thioglycolic acid towards super photocatalysis performance. *J. Alloys Compd.* **2019**, 780, 660-670.
(38) Lin, L.; Feng, X.; Lan, D.; Chen, Y.; Zhong, Q.; Liu, C.; Cheng, Y.; Qi, R.; Ge, J.; Yu, C.; Duan, C.-G.; Huang, R. Coupling effect of Au nanoparticles with the oxygen vacancies of TiO_{2-x} for enhanced charge transfer. *J. Phys. Chem. C* **2020**, 124, 23823-23831.
(39) Huang, Z.; Wu, P.; Gong, B.; Zhang, X.; Liao, Z.; Chiang, P.-C.; Hu, X.; Cui, L. Immobilization of visible light-sensitive (N, Cu) co-doped TiO_2 onto rectorite for photocatalytic degradation of p-chlorophenol in aqueous solution. *Appl. Clay Sci.* **2017**, 142, 128-135.
(40) Tahir, M.; Tahir, B. Dynamic photocatalytic reduction of CO_2 to CO in a honeycomb monolith reactor loaded with Cu and N doped TiO_2 nanocatalysts. *Appl. Surf. Sci.* **2016**, 377, 244-252.
(41) Mai, J.; Fang, Y.; Liu, J.; Zhang, J.; Cai, X.; Zheng, Y. Simple

DOI: 10.14102/j.cnki.0254-5861.2022-0191

synthesis of WO_3-Au composite and their improved photothermal synergistic catalytic performance for cyclohexane oxidation. *Mol. Catal.* **2019**, 473, 110389.

(42) Wu, Q.; Li, Z.; Zhang, X.; Huang, W.; Ni, M.; Cen, K.; Zhang, Y. Enhanced defect-water hydrogen evolution method for efficient solar utilization: photo-thermal chemical coupling on oxygen vacancy. *Chem. Eng. J.* **2021**, 408, 127248.

(43) Li, F.; Yue, X.; Zhang, D.; Fan, J.; Xiang, Q. Targeted regulation of exciton dissociation in graphitic carbon nitride by vacancy modification for efficient photocatalytic CO_2 reduction. *Appl. Catal., B* **2021**, 292, 120179.

(44) Han, C.; Zhang, R.; Ye, L.; Wang, L.; Ma, Z.; Su, F.; Xie, H.; Zhou, Y.; Wong, P. K.; Ye, L. Chainmail co-catalyst of NiO shell-encapsulated Ni for improving photocatalytic CO_2 reduction over g-C_3N_4. *J. Mater. Chem. A* **2019**, 7, 9726-9735.

(45) Jiang, Z.; Sun, H.; Wang, T.; Wang, B.; Wei, W.; Li, H.; Yuan, S.; An, T.; Zhao, H.; Yu, J.; Wong, P. K. Nature-based catalyst for visible-light-driven photocatalytic CO_2 reduction. *Energy Environ. Sci.* **2018**, 11, 2382-2389.

(46) He, Y.; Li, C.; Chen, X.-B.; Shi, Z.; Feng, S. Visible-light-responsive UiO-66(Zr) with defects efficiently promoting photocatalytic CO_2 reduction. *ACS Appl. Mater. Interfaces* **2022**, 14, 28977-28984.

(47) Jin, L.; Shaaban, E.; Bamonte, S.; Cintron, D.; Shuster, S.; Zhang, L.; Li, G.; He, J. Surface basicity of metal@TiO_2 to enhance photocatalytic efficiency for CO_2 reduction. *ACS Appl. Mater. Interfaces* **2021**, 13, 38595-38603.

(48) Yang, P.; Wang, R.; Zhuzhang, H.; Titirici, M.-M.; Wang, X. Photochemical construction of nitrogen-containing nanocarbons for carbon dioxide photoreduction. *ACS Catal.* **2020**, 10, 12706-12715.

(49) Chen, C.; Wang, T.; Yan, K.; Liu, S.; Zhao, Y.; Li, B. Photocatalytic CO_2 reduction on Cu single atoms incorporated in ordered macroporous TiO_2 toward tunable products. *Inorg. Chem. Front.* **2022**, 9, 4753-4767.

(50) Li, N.; Wang, B.; Si, Y.; Xue F.; Zhou, J.; Lu, Y.; Liu, M. Toward high-value hydrocarbon generation by photocatalytic reduction of CO_2 in water vapor. *ACS Catal.* **2019**, 9, 5590-5602

(51) Wang, Y.; Tang, X.; Huo, P.; Yan, Y.; Zhu, Z.; Dai, J.; Liu, Z.; Li, Z.; Xi, H. Insight into the effect of the Cl 3p orbital on g-C_3N_4 mimicking photo-synthesis under CO_2 reduction. *J. Phys. Chem. C* **2021**, 125, 9646-9656.

(52) Kang, S.; Li, Z.; Xu, Z.; Zhang, Z.; Sun, J.; Bian, J.; Bai, L.; Qu, Y.; Jiang, L. Synthesis of mixed-valence Cu phthalocyanine/graphene/g-C_3N_4 ultrathin heterojunctions as efficient photocatalysts for CO_2 reduction. *Catal. Sci. Technol.* **2022**, 12, 4817-4825.

(53) Huang, Z.; Wu, J.; Ma, M.; Wang, J.; Wu, S.; Hu, X.; Yuan, C.; Zhou, Y. The selective production of CH_4 via photocatalytic CO_2 reduction over Pd-modified BiOCl. *New J. Chem.* **2022**, 46, 16889-16898.

(54) Su, F.; Chen, Y.; Wang, R.; Zhang, S.; Liu, K.; Zhang, Y.; Zhao, W.; Ding, C.; Xie, H.; Ye, L. Diazanyl and SnO_2 bi-activated g-C_3N_4 for enhanced photocatalytic CO_2 reduction. *Sustain. Energy Fuels* **2021**, 5, 1034-1043.

Received: September 26, 2022
Accepted: October 7, 2022
Published online: October 11, 2022
Published: December 2, 2022

DOI: 10.14102/j.cnki.0254-5861.2022-0191